sciendo

PRODUCTION ENGINEERING ARCHIVES 2023, 29(1), 94-100

PRODUCTION ENGINEERING ARCHIVES

ISSN 2353-5156 (print)
ISSN 2353-7779 (online)

Exist since 4th quarter 2013
Available online at www.pea-journal.eu

Properties of WC-Co coatings with Al_2O_3 addition

Norbert Radek[1*]

[1] Kielce University of Technology, al. 1000-lecia P.P. 7, 25-314 Kielce, Poland
*Corresponding author e-mail: norrad@tu.kielce.pl

Received 04.10.2022
Accepted 20.12.2022
Available online 20.02.2023

Keywords
mild steel
electrospark deposition
WC-Co-Al_2O_3 coating
properties
corrosion resistance

Abstract
Properties of WC-Co coatings with Al_2O_3 addition on the C45 mild steel surface in acidic chloride solution were examined. The WC-Co-Al_2O_3 coatings on steel surfaces were deposited by an electrospark (ESD) technique. The anti-corrosion properties of the coatings were mainly investigated by electrochemical methods. Moreover, the scanning electron microscope (SEM) was employed for the observation of the surface of materials. The structure of coatings depended on the composition of electrospark electrodes. In the WC80-Co5-$Al_2O_3$15 coating, the largest corrosion resistance was shown. The corrosion rate of the specimen was approximately eight times smaller than the coating without of Al_2O_3 addition. The aim of the research was to obtain, by adding alumina, an improvement in the functional properties of WC-Co coatings produced by the ESD method. Due to the original features of ESD coatings, they can be used in sliding friction pairs and as anti-wear coatings on cutting tools.

DOI: 10.30657/pea.2023.29.11

1. Introduction

Carbon and mild steel are very widely used, mainly as construction materials in a wide range of industries. The corrosion of steel surfaces in acidic solutions contributes to considerable costs. In order to reduce the corrosion of metals, several techniques have been applied (Badawi et al., 2010; Solmaz, 2010). The electrospark deposition (ESD) process has drawn increasing attention as a promising surface treatment technique. Electrospark deposition is a low-cost and effective method for improving the performance characteristics of metal parts. The defects of ESD coatings can be eliminated using, among others, laser treatment (Radek et al., 2018). Metal coatings deposited on the metal substrates improve the corrosion resistance of the latter contributing to the improvement of the operating life of different metal parts (Radek et al., 2021). The deposition of the coating by means of ESD involves the use of spark discharge energy to carry the mass of the material being eroded from the carefully selected electrode (anode), which provides the coating material, to the negative electrode (the cathode), which constitutes a specially modified substrate.

The quality of electrospark deposition mainly depends on the shape, the duration, and the average value of current or pulse power.

Sintered carbides are cermets consisting of 70÷96% refractory metal (e.g. tungsten, tantalum, niobium) carbides and a binding matrix that is usually cobalt, sometimes molybdenum or nickel, and occasionally iron. Presently, sintered carbides are a very popular material for making cutting tool edges, especially in turning and milling operations (http://www.fanar.pl).

The use of ceramic tool materials is low when compared with sintered carbides, yet it tends to grow continually. It is estimated that approx. 5% of cutting tool edges are made of this material type. The substances most widely used to manufacture ceramic tool materials include the following:

- single-phase alumina Al_2O_3,
- silicon nitride Si_3N_4,
- multi-phase Al_2O_3 and Si_3N_4 mixtures with hard carbides, nitrides, and oxides.

An interesting option is provided by the manufacture of anti-wear carbide-ceramic coatings that are electrospark deposited using electrodes obtained by powder metallurgy (Konstanty, 2005; Chang-bin et al., 2011; Salmaliyan et al., 2017). Super-hard coatings can be deposited on the edges of cutting tools, such as e.g. lathe tools, milling cutters, pinion cutters, or taps. It is supposed that the coatings of concern can be successfully applied to those machine components that operate under extreme conditions, including high abrasive wear or impact loads.

Another advantage offered by super-hard electrospark deposited coatings concerns their low environmental impact. Electrospark machining does not produce a harmful ecological

effect, so it should be accounted for in environmental research (Bielski, 2021; Maltsevich, 2021; Wójcicka, 2021).

Highly wear-resistant materials have a very wide range of applications, from biotechnological equipment (Skrzypczak-Pietraszek et al., 2018; Skrzypczak-Pietraszek et al., 2019), through intelligent in civil engineering (Piotrowski et al., 2014; Majewski et al., 2020) and classic reinforcement of mechanically (Dwornicka et al., 2017; Radek et al., 2018; Markovic et al., 2021) and thermo-mechanically cooperating machine parts (Orman, 2014; Dabek et al., 2019; Orman et al., 2020), to production engineering (Pacana et al., 2014; Pacana et al., 2019; Pacana et al., 2020). The study of the properties of such reinforced materials is an intense subject of work in materials science (Ulewicz, 2015; Radzyminska-Lenarcik et al., 2018) and inspiration for data analysis methods (Styrylska and Pietraszek, 1992), both classical (Pietraszek et al., 2014) and non-parametric approaches: fuzzy (Pietraszek, 2012), neural-network-based (Pietraszek, 2003; Regulski and Abramek, 2022) and resampling (Pietraszek and Gadek-Moszczak, 2013).

The promising results should also be inspiring for other mechanical applications (Czyczuła and Rochel, 2021; Radzajewski, 2021; Kurp and Danielewski, 2022)

The aim of the current investigations concerned the influence composition of electrospark electrodes on the corrosion resistance of WC-Co-Al_2O_3 coatings on the C45 mild steel surface. The aggressive acidic chloride environment was used for the testing of the corrosion resistance of materials. The study mainly applied an electrochemical method.

2. Experimental

The WC-Co or WC-Co-Al_2O_3 coatings were produced by electrospark deposition. Cylindrical electrospark electrodes, 5 mm in diameter and 40 mm in height, were used to deposit the coatings on the C45 mild steel surface. Table 1 shows the chemical composition of C45 mild steel, while Table 2 shows elemental composition of electrospark electrodes.

Table 1. Chemical composition of C45 mild steel

Elements	C	Mn	Si	P	S
Content, %	0.42-0.50	0.50-0.80	0.10-0.40	0.04	0.04

Table 2. Mixture nanopowders and elemental composition of electrospark electrodes/coatings

Electrospark electrode symbol	Mixture nanopowders	Elemental electrospark electrode/coating composition
EA	80% WC, 20% Co	WC80-Co20
EB	80% WC, 15% Co, 5% Al_2O_3	WC80-Co15-$Al_2O_3$5
EC	80% WC, 10% Co, 10% Al_2O_3	WC80-Co10-$Al_2O_3$10
ED	80% WC, 5% Co, 15% Al_2O_3	WC80-Co5-$Al_2O_3$15

They were produced by the impulse-plasma sintering method in a graphite matrix of tungsten carbide (particle diameter ~0,2 μm, OMG (USA)), metallic cobalt (particle diameter ~0.4 μm, Umicore (Belgium)) and aluminum oxide (particle diameter ~0.15 μm, SNI (USA)) nanopowders at the temperature of 1100 °C, under the pressure of 50 MPa. The nanopowders: WC, Co, and Al_2O_3, were mixed in the appropriate proportions, which are listed in Table 2.

Images of the electrospark electrodes of WC80-Co20 and WC80-Co15-$Al_2O_3$5, respectively, are shown in Figure 1.

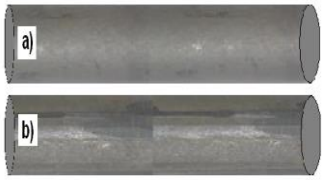

Fig. 1. Image of the electrospark electrodes: a) WC80-Co20 (EA), and b) WC80-Co15-$Al_2O_3$5 (EB). Magnification ×10

An EIL-8A pulse spark generator was used to deposit coatings on the steel surface. The maximum output power of the electrospark deposition welder was 4 kW, with a voltage output of 250 V (50 Hz) continuously regulated and eight-step capacitance (470 μF). The revolving electrospark electrode was held on the deposition gun that rotates around its own axis at the speed of 240 circles/minute during the work time.

The surface topography of the specimen was observed using a scanning electron microscope (SEM) Joel, type JSM-5400. The accelerating voltage was 20 kV. Figure 2 shows the SEM image of the top surface of C45 mild steel after mechanical treatment and WC80-Co10-$Al_2O_3$10 coating on the steel surface. A similar surface was obtained for the remaining specimens of WC-Co-Al_2O_3 coatings.

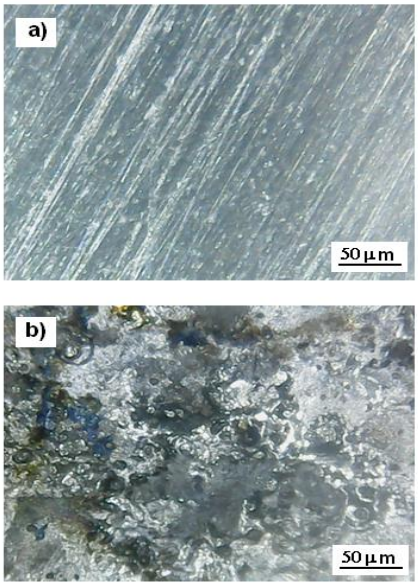

Fig. 2. SEM image of the top surface: a) C45 mild steel after mechanical treatment, and b)WC80-Co10-$Al_2O_3$10 coating on the steel surface

The scratches visible on the steel surface are the result of mechanical treatment (Fig. 2a). The splash appearance, microcracks, and spattering particles can be seen (Fig. 2b). Molten droplets formed on the electrode tip during the heating process. The droplets are accelerated by high current plasma and impinge on the substrate surface resulting in the splash in different directions. Moreover, the elemental composition of all coatings is very similar to the initial composition of the electrospark electrode used (Table 2).

All electrochemical measurements were made using a potentiostat/galvanostat PGSTAT 128N, AutoLab, Netherlands, with the NOVA 1.7 software of the same producer. The corrosion tests were performed with a conventional three-electrode cell. Potentiodynamic polarization curves were recorded in a 1.2 M hydrochloric acid solution. Measurements were carried out in the potential range from -800 to -50 mV vs. SCE. The potential scan rate in all experiments was 1 mV s^{-1}. Potentiodynamic polarization curves were used to designate the corrosion potential (E_{corr}) and corrosion current density (j_{corr}). Extrapolation of Tafel lines is one of the most popular DC techniques for the estimation of corrosion rate. The extrapolation of anodic and/or cathodic Tafel lines for charge transfer controlled reaction gives the E_{corr} and j_{corr} at the corrosion potential. All measurements were carried out at the temperature of 25 ±0.5 ^{0}C, which was maintained by an air thermostat of home production. The experiment was started 30 min. after immersing the electrode in the testing solution, which was neither mixed nor deoxidized. Each test was repeated three times to verify the reproducibility of data, and the average values were reported.

An analysis of the phase composition of WC-Co or WC-Co-Al_2O_3 coating was carried out by means of the X-ray diffraction method using a Philips PW 1830 spectrometer equipped with a copper anode tube powered with a voltage of 40 kV and a current of 30 mA. During the measurement, the 2Θ angle was changed in the range of 40^0-80^0, and the scanning velocity of 0.05^0/3 seconds.

Microhardness values of the studied specimens were determined by the Vickers (HV) method using a Microtech MX3 tester under the load of 0.4 N.

3. Results and discussion

3.1. Microstructure and X-ray diffraction analysis

The element distribution of the cross-section map of WC80-Co15-$Al_2O_3$5 coating on C45 mild steel is shown in Figure 3. The uniform distribution of elements can be observed, indicating that the alloying process of the elements was fully performed between the base and the substrate. In addition, Co and Al_2O_3 transfer to the substrate so easily that it is difficult to recognize the interface between the substrate and the coating according to both material's face distribution map (Fig. 3).

Figure 4a represents the cross-section image of WC80-Co15-$Al_2O_3$5 of electrospark coating on the C45 mild steel surface, which was observed by a scanning electron microscope. It is clear that the thickness of the obtained layers was from 34 to 64 μm, whereas the heat affected zone (HAZ) ranged approximately from 23 to 31 μm into the substrate. Figure 6 also reveals a clear boundary between the coating and the substrate, pores, and microcracks.

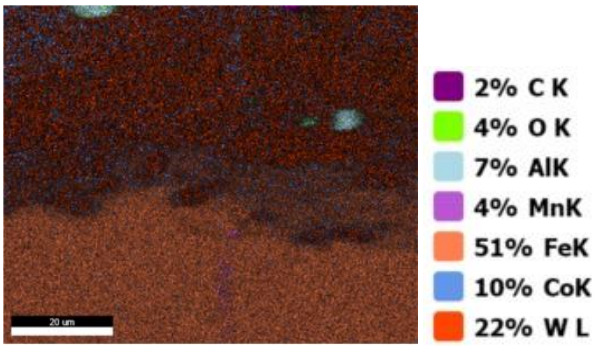

Fig. 3. Element distribution of the cross-section map WC80-Co15-$Al_2O_3$5 coating on C45 mild steel

The EDX analysis of the coating is illustrated in Figure 4b. The presence of WC, Co, C, Al, and Fe elements proves the alloy formation between the coating and the substrate. As can be seen, the coating surface is characterized as an irregular and rough view due to the globular mass transfer mechanism during the ESD process from the electrode to the substrate. The analysis of the microstructure and other functional properties of the WC-Co-Al_2O_3 coatings was carried out in the papers (Radek and Bartkowiak, 2010; Radek et al., 2014).

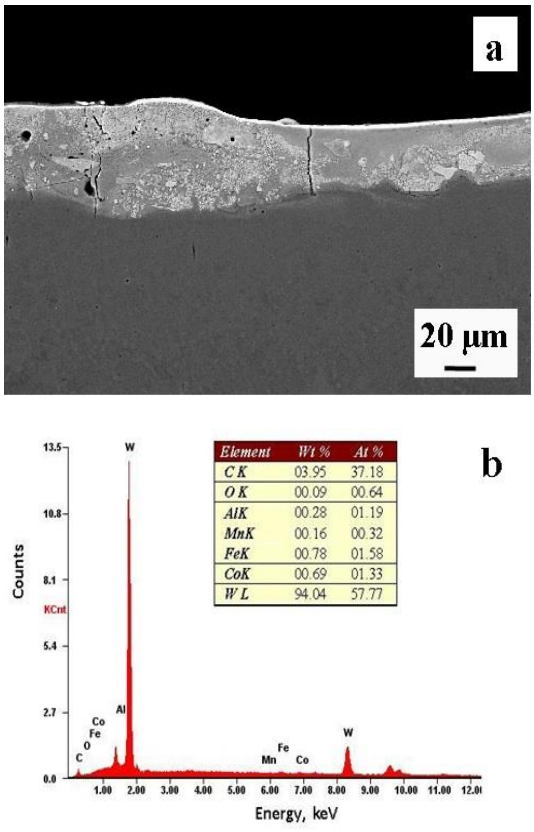

Fig. 4. The morphology (a) and EDX analysis (b) of the WC80-Co15-$Al_2O_3$5 coating surface obtained by using the ESD process

As shown in X-ray diffraction analysis (Fig. 5), the superficial layer of the coating consists of WC and W_2C as well as a small amount of Co_2C and Al_2O_3. W_2C is known to appear as an intermediate during the formation and dissolution of WC. Besides, it has been found that peaks from the W_2C phase are the most intense.

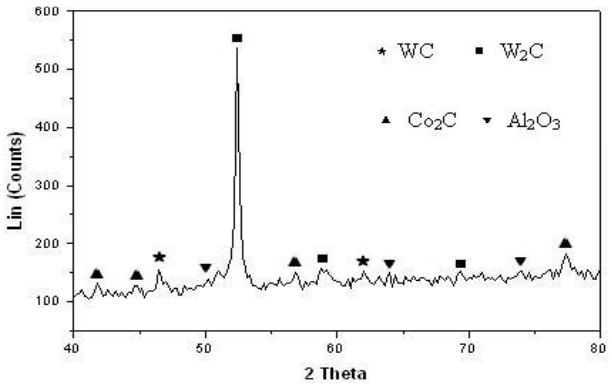

Fig. 5. X-ray diffraction pattern of the WC80-Co15-$Al_2O_3$5 coating

3.2. Properties of materials

Table 2 shows the results of microhardness measurements, thickness, and roughness of ESD coatings. The microhardness of the specimens with coatings was analyzed by applying a load of 0.4 N and using the Vickers method. The microhardness is listed in Table 3 as an average value of 15 points on the surface of each coating.

Table 3. Characteristics of ESD coatings

Coating	Average microhardness HV0.4	Average thickness, µm	Average roughness Ra, µm
C45 mild steel	278 ± 11	–	0.51
WC80-Co20	794 ± 26	52	4.98
WC80-Co15-$Al_2O_3$5	883 ± 54	49	5.26
WC80-Co10-$Al_2O_3$10	938 ± 37	47	5.34
WC80-Co5-$Al_2O_3$15	1042 ± 41	51	5.63

The indentations were made consecutively in three zones: the coating, the heat-affected zone (HAZ), and the base material. The average microhardness of the base material after ESD was 278 HV0.4. The value was the same as that at the initial state. It follows that the lower value of microhardness (794 HV0.4) belongs to the WC80-Co20 coating. The WC80-Co5-$Al_2O_3$15 coating has the highest microhardness, about 1042 HV0.4. The average microhardness of the WC80-Co15-$Al_2O_3$5 coating was 883 HV0.4. Thus, there was a 218 percent increase compared to that of the base material. The microhardness of the heat-affected zone after the electrospark deposition was 38% higher in relation to that of the base material. The average thickness of ESD coatings was between 47 and 52 µm.

The roughness of the coatings was measured at the Laboratory for Measurement of Geometric Quantities of the Kielce University of Technology using TALYSURF CCI equipment. The roughness was measured in two directions perpendicular to each other. Then, the average values of coatings were calculated: Ra = 4.98-5.63 µm. The without coatings steel specimens (C45 mild steel) had a roughness from 0.47 to 0.54 µm.

3.3. Potentiodynamic polarization curves

The generation of polarization curves continues to be important in aqueous corrosion research. The time-consuming potentiostatic method has been largely replaced by the potentiodynamic approach, where the potential of the corroding metal is automatically varied with time. Moreover, the current need to maintain the metal at each applied potential is ascertained, and the potential/current data are plotted to give the experimental polarization curve. Figure 6 shows a typical example of potentiodynamic polarization curves for C45 mild steel without and with of WC-Co or WC-Co-Al_2O_3 coatings in a 1.2 M solution of chlorides. Tungsten carbide (WC), cobalt (Co), and aluminum oxide (Al_2O_3) were mixed in various proportions. Figure 6, curve (a) depicts the uncoated C45 mild steel electrode, while curves (b) - (e) correspond to the electrodes with of WC-Co or WC-Co-Al_2O_3 coatings, respectively.

For C45 mild steel and of WC-Co or WC-Co-Al_2O_3 coatings in the acidic chloride environment, the cathode branches correspond to the reduction reaction of hydrogen:

$$Fe + 2\,H^+ \rightarrow Fe + H_2 - 2\,e^- \quad (1)$$

The metal surface is typically not affected during cathodic polarization as it is cathodically protected, although in an acid solution, hydride formation may change its characteristics. The hydrogen reduction reaction itself, and especially at higher rates, may change the solution characteristics at the interface by, for instance, screening with hydrogen bubbles, enhancing mass transfer due to the micro-stirring caused by gas evolution, and changing the hydrogen ion activity at the interface (Sandenbergh et al., 2005).

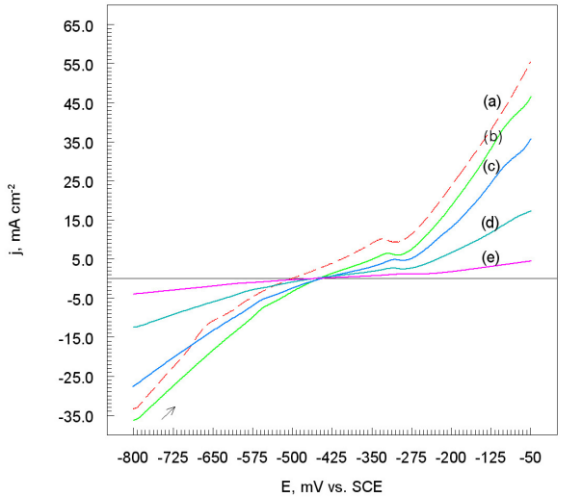

Fig. 6. Potentiodynamic polarization curves for C45 mild steel: a) without coating and with, b) WC80-Co20, c) WC80-Co15-$Al_2O_3$5, d) WC80-Co10-$Al_2O_3$10, e) WC80-Co5-$Al_2O_3$15 coatings. Solution contained 1.2 M Cl^-, dE/dt 1mV s^{-1} at 25 ^{0}C

When the potential of the electrode changed in the anodic direction, the adsorption layer on the electrode surface appeared:

$$Fe + Cl^- + H_2O \rightarrow (FeClOH)_{ads} + H^+ + 2\,e^- \quad (2)$$

The layer of $(FeClOH)_{ads}$ appears on the surface of the electrode at a potential of about -340 mV vs. SCE (Fig. 6, curve (a)). The $(FeClOH)_{ads}$ layer partially protects the C45 mild steel surface against oxidation in the chloride environment. Unfortunately, the $(FeClOH)_{ads}$ layer in the acidic solution was dissolved, according to the reaction:

$$(FeClOH)_{ads} + H^+ \rightarrow Fe^{2+} + Cl^- + H_2O \quad (3)$$

The acidic chloride electrolyte was not deoxidized; therefore, the next anodic reaction of the steel electrode was as follows:

$$Fe + 3\,H^+ + 3/2\,O_2 \rightarrow FeOOH + H_2O + 9\,e^- \quad (4)$$

The electrode surface was coated with a porous iron oxide layer according to the reaction:

$$2\,FeOOH \rightarrow Fe_2O_3 + H_2O \quad (5)$$

However, the authors (Balaban et al., 2004; Singh et al., 2010) suggested a similar mechanism of corrosion of steel in an acidic chloride environment.

Furthermore, the inhibition corrosion process of the C45 mild steel surface with WC80-Co20 coating was also associated with the sealing of the cobalt layer due to the adsorption of the reaction product:

$$Co + Cl^- \rightarrow (CoCl)_{ads} + e^- \quad (6)$$

However, for more positive potentials (Fig. 8, curve (b)) of the working electrode follows the dissolving of the layer:

$$(CoCl)_{ads} \rightarrow Co^+ + Cl^- \quad (7)$$

Therefore, the process corrosion of C45 mild steel as substrate with of WC80-Co20 coating does not slow down. Similarly, Cl^- ion is adsorbed onto the copper surface.

Potentiodynamic polarization curves for WC-Co-Al_2O_3 coatings are presented in Fig. 6, curves (c) – (e). It has been found that the cathodic and anodic current density decreases as the Al_2O_3 content on the WC-Co-Al_2O_3 coatings increases. Probably, in the acidic environment of chlorides at the boundary of both phases, a simple chemical reaction occurs:

$$Al_2O_3 + 4\,H^+ + 4\,Cl^- \rightarrow 2\,[Al(OH)Cl_2]_{ads} + H_2O \quad (8)$$

The $[Al(OH)Cl_2]_{ads}$ layer additionally protects the C45 mild steel surface against corrosion in the chloride environment. Moreover, the $[Al(OH)Cl_2]_{ads}$ layer thickness is the biggest in the case of WC80-Co5-$Al_2O_3$15 coating (Fig. 6, curve (e)). Therefore, the WC-Co-Al_2O_3 coatings effectively protect the C45 mild steel surface against corrosion in aggressive environments.

Potentiodynamic polarization curves (Fig. 6) were used to determine various parameters of metal corrosion which were summarized in Table 4.

In the case of WC-Co or WC-Co-Al_2O_3 coatings, the corrosion potential shifted slightly towards negative values The corrosion current density decreased as a result of the high Al_2O_3 (15%) content in the mixture of nanopowders (Table 4). The polarization curves (Fig. 6) show that WC-Co-Al_2O_3 coatings have an effect on anodic slopes and suppress anodic processes only. Thus, the increase in Al_2O_3 content influences on the change in the iron oxidation mechanism. The polarization resistance values were calculated according to Eq. (Poorqasemi et al., 2009) and are listed in Table 4. An increase in R_p values for WC-Co-Al_2O_3 coatings means that Al_2O_3 addition to WC-Co nanopowders (Table 2) significantly reduces the exchange of mass and electric charge between the electrode and the electrolyte ions.

The results show also that the mechanism of the anodic dissolution of iron depends on the elemental composition of the coat.

Table 4. Corrosion parameters and polarization resistance for C45 mild steel in the absence and with the presence of WC-Co or WC-Co-Al_2O_3 coatings at 25 ^{0}C

Coating	E_{corr},	j_{corr},	$-b_c$,	b_a,	R_p,
	mV	mA cm^{-2}	mV dec^{-1}		Ω cm^2
Absence	-498	1.78	160	190	21
WC80-Co20	-449	1.48	145	180	24
WC80-Co15-$Al_2O_3$5	-443	0.89	135	170	37
WC80-Co10-$Al_2O_3$10	-456	0.49	140	240	78
WC80-Co5-$Al_2O_3$15	-452	0.19	155	255	220

3.4. Surface images

Figure 10 shows the images of the top surface of C45 mild steel with WC80-Co20, WC80-Co15-$Al_2O_3$5, WC80-Co10-$Al_2O_3$10, and WC80-Co5-$Al_2O_3$15 coatings, after exposure of specimens for 360 hours in 1.2 M Cl^-.

Figure 7a shows of the top surface of C45 mild steel with WC80-Co20 coating after exposure for 360 hours in 1.2 M Cl^-. It can be observed that the specimen surface was partially damaged (reactions (2) – (5)), but still, the WC80-Co20 coating adheres to the steel surface. Figure 7b and 7c present the specimen surface with WC80-Co15-$Al_2O_3$5 and WC80-Co10-$Al_2O_3$10 coatings. It is noteworthy that on the surface of both specimens, there are no visible corrosion products of iron. It is clear that the addition of Al_2O_3 to WC and Co powders results in a significant improvement in the anti-corrosive properties of WC-Co coatings. In the case of coating the WC80-Co5-$Al_2O_3$15 (Fig. 7d)) the surface of the specimen is tightly

covered by Al_2O_3. Therefore, the aggressive chloride solution does not penetrate the substrate, and no corrosion products are visible of WC80-Co5-$Al_2O_3$15 on the surface of the specimen.

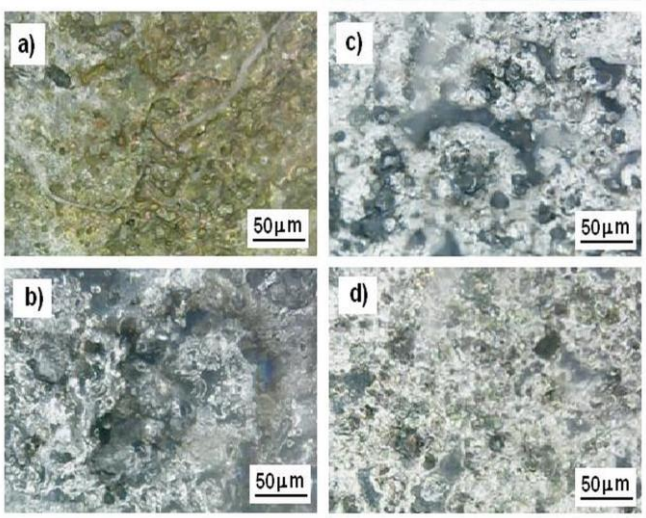

Fig. 7. Images of the top surface of C45 mild steel with: a) WC80-Co20,b) WC80-Co15-$Al_2O_3$5, c) WC80-Co10-$Al_2O_3$10, and d) WC80-Co5-$Al_2O_3$15 coatings. After exposure for 360 hours in 1.2 M Cl^-

4. Conclusions

On the basis of the study, it was found that:

1. Electrospark deposition (ESD) using WC-Co or WC-Co-Al_2O_3 electrodes can produce anti-wear coatings on the surface of C45 mild steel.
2. The content of Al_2O_3 in the mixture of electrospark nanopowders clearly improves the anti-corrosion properties of the WC-Co coating by about two to eight times.
3. The polarization resistance of the C45 mild steel substrate with WC80-Co20 coating was much bigger (about eight times) compared to the WC80-Co5-$Al_2O_3$15 coating.
4. The microstructure analysis revealed that the coating thickness was 47-52 µm, whereas the heat-affected zone ranged from approximately 20-33 µm. The coatings possessed microcracks and small amounts of pores.
5. The microhardness of the coatings produced by the electrospark deposited was 794-1042 HV0.4, while that of the base material - C45 mild steel - was 278 HV0.4.
6. The coating surface is composed of WC and W_2C, besides a small amount of Co_2C and Al_2O_3.

Reference

Badawi, A.M., Hegazy, M.A., El-Sawy, A.A., Ahmed, H.M., Kamel, W.M., 2010. Novel quaternary ammonium hydroxide cationic surfactants as corrosion inhibitors for carbon steel and as biocides for sulfate reducing bacteria (SRB). Mat. Chem. Phys., 124, 458-465.

Balaban, Y.A., Kandemir, S.U., 2004. Investigation on some schiff bases as HCl corrosion inhibitors for carbon steel. Mater. Chem. Phys., 85, 420-426.

Bielski, A., 2021. Mixing effects in the river downstream from pollution discharge point. Technical Transactions 118, art. e2021004, DOI: 10.37705/TechTrans/e2021004

Chang-bin, T., Dao-xin, L., Zhan, W., Yang, G., 2011. Electro-spark alloying using graphite electrode on titanium alloy surface for biomedical applications. Appl. Surf. Sci., 257, 6364-6371.

Czyczuła,W, Rochel, M., 2021. Operational problems of tramway infra-structure in sharp curves. Technical Transactions 118, art. e2021015. DOI: 10.37705/TechTrans/e2021015

Dabek, L., Kapjor, A. Orman, L.J., 2019. Distilled water and ethyl alcohol boiling heat transfer on selected meshed surfaces. Mechanics & Industry, 20, art. 701, DOI: 10.1051/meca/2019068

Dwornicka, R., Radek, N., Krawczyk, M., Osocha, P., Pobedza, J., 2017. The laser textured surfaces of the silicon carbide analyzed with the bootstrapped tribology model. METAL 2017 26th Int. Conf. Metallurgy and Materials, Ostrava, Tanger, 1252-1257

http://www.fanar.pl [on-line access 07.09.2022].

Konstanty, J., 2005. Powder metallurgy diamond tools. Elsevier, Oxford.

Kurp P, Danielewski H., 2022. Metal expansion joints manufacturing by a mechanically assisted laser forming hybrid method – concept. Technical Transactions 119, art. e2022008, DOI: 10.37705/TechTrans/e2022008

Majewski, G., Orman, L.J., Telejko, M., Radek, N., Pietraszek, J., Dudek, A., 2020. Assessment of Thermal Comfort in the Intelligent Buildings in View of Providing High Quality Indoor Environment. Energies, 13, art. 1973, DOI: 10.3390/en13081973

Maltsevich, I., 2021. Technological structures in construction during the implementation of the National Strategy for Sustainable Development – 2035. Construction of Optimized Energy Potential, 10(2), 61-68, DOI: 10.17512/bozpe.2021.2.08

Markovic, S., Arsic, D., Nikolic, R.R., Lazic, V., Hadzima, B., Milovanovic, V.P., Dwornicka, R., Ulewicz, R., 2021. Exploitation Characteristics of Teeth Flanks of Gears Regenerated by Three Hard-Facing Procedures. Materials, 14(15), art. 4203, DOI: 10.3390/ma14154203

Orman, Ł.J., 2014. Boiling heat transfer on single phosphor bronze and copper mesh microstructures. EFM13 – Experimental Fluid Mechanics, 67, art. 2087, DOI: 10.1051/epjconf/20146702087

Orman, L.J., Radek, N., Pietraszek, J., Szczepaniak, M., 2020. Analysis of Enhanced Pool Boiling Heat Transfer on Laser-Textured Surfaces. Energies, 2020, art. 2700, DOI: 10.3390/en13112700

Pacana, A., Czerwinska, K., Dwornicka, R., 2019. Analysis of non-compliance for the cast of the industrial robot basis. METAL 2019 28th Int. Conf. Metallurgy and Materials, Ostrava, Tanger, 644-650, DOI: 10.37904/metal.2019.869

Pacana, A., Gazda, A., Malindzak, D., Stefko, R., 2014. Study on improving the quality of stretch film by Shainin method. Przemysł Chemiczny, 93, 243-245.

Pacana, A., Siwiec, D., Bednarova, L., 2020. Method of Choice: A Fluorescent Penetrant Taking into Account Sustainability Criteria. Sustainability, 12, art. 5854, DOI: 10.3390/su12145854

Pietraszek, J., 2003. Response surface methodology at irregular grids based on Voronoi scheme with neural network approximator. Neural Networks and Soft Computing, 19, 250-255, DOI: 10.1007/978-3-7908-1902-1_35

Pietraszek, J., 2012. Fuzzy Regression Compared to Classical Experimental Design in the Case of Flywheel Assembly. Artificial Intelligence and Soft Computing, 7267, 310-317, DOI: 10.1007/978-3-642-29347-4_36

Pietraszek, J., Gądek-Moszczak, A., 2013. The Smooth Bootstrap Approach to the Distribution of a Shape in the Ferritic Stainless Steel AISI 434L Powders. Solid State Phenomena, 197, 162-167, DOI: 10.4028/www.scientific.net/SSP.197.162

Pietraszek, J., Gądek-Moszczak, A., Toruński, T., 2014. Modeling of Errors Counting System for PCB Soldered in the Wave Soldering Technology. Advanced Materials Research, 874, 139-143, DOI: 10.4028/www.scientific.net/AMR.874.139

Piotrowski, J.Z., Orman, L.J., Lucas, X. Zender-Swiercz, E., Telejko, M., Koruba, D., 2014. Tests of thermal resistance of simulated walls with the reflective insulation. EFM13 - Experimental Fluid Mechanics, 67, art. 2095, DOI: 10.1051/epjconf/20146702095

Poorqasemi, E., Abootalebi, O., Peikari, M., Haqdar, F., 2009. Investigating accuracy of the Tafel extrapolation method in HCl solutions. Corros. Sci., 51, 1043-1054.

Radek, N., Bartkowiak, K., 2010. Performance properties of electro-spark deposited carbide-ceramic coatings modified by laser beam. Physics Procedia, 5, 417-423.

Radek, N., Konstanty, J., Pietraszek, J., Orman, Ł.J., Szczepaniak, M., Przestacki, D., 2021. The effect of laser beam processing on the properties of WC-Co coatings deposited on steel. Materials, 14, 538.
Radek, N., Sladek, A., Bronček, J., Bilska, I., Szczotok, A., 2014. Electro-spark alloying of carbon steel with WC-Co-Al_2O_3: deposition technique and coating properties. Advanced Materials Research, 874, 101-106.
Radek, N., Szczotok, A., Gądek-Moszczak, A., Dwornicka, R., Bronček, J., Pietraszek, J., 2018. The impact of laser processing parameters on the properties of electro-spark deposited coatings. Archives of Metallurgy and Materials, 63, 809-816, DOI:10.24425/122407
Radzajewski, P., 2021. Calculation of brake-force distribution on three-axle agricultural trailers using simulation methods. Technical Transactions 118, art. e2021029, DOI: 10.37705/TechTrans/e2021029
Radzyminska-Lenarcik, E., Ulewicz, R., Ulewicz, M., 2018. Zinc recovery from model and waste solutions using polymer inclusion membranes (PIMs) with 1-octyl-4-methylimidazole. Desalination and Water Treatment, 102, 211-219, DOI: 10.5004/dwt.2018.21826
Regulski, P, Abramek, K., 2022. The application of neural networks for the life-cycle analysis of road and rail rolling stock during the operational phase. Technical Transactions 119, art. e2022002. DOI: 10.37705/TechTrans/e2022002
Salmaliyan, M., Malek-Ghaeni, F., Ebrahimnia, M., 2017. Effect of electro spark deposition process parameters on WC-Co coating on H13 steel. Surf. Coat. Tech., 321, 81-89.
Sandenbergh, R.F., Van der Lingen, E., 2005. The use of Tafel back extrapolation to clarify the influence of ruthenium and palladium alloying on the corrosion behaviour of titaniumin concentrated hydrochloric acid. Corros. Sci., 47, 3300-3311.
Singh, A.K., Quraishi, M.A., 2010. Investigation of adsorption of ionized derivatives at mild steel/hydrochloric acid interface: Electrochemical and weight loss methods. Mater. Chem. Phys., 123, 666-677.
Skrzypczak-Pietraszek, E., Reiss, K., Zmudzki, P., Pietraszek, J., 2018. Enhanced accumulation of harpagide and 8-O-acetyl-harpagide in Melittis melissophyllum L. agitated shoot cultures analyzed by UPLC-MS/MS. PLoS ONE, 13, art. e0202556, DOI: 10.1371/journal.pone.0202556
Skrzypczak-Pietraszek, E., Urbanska, A., Zmudzki, P., Pietraszek, J., 2019. Elicitation with methyl jasmonate combined with cultivation in the Plantform (TM) temporary immersion bioreactor highly increases the accumulation of selected centellosides and phenolics in Centella asiatica (L.) Urban shoot culture. Engineering in Life Sciences, 19, 931-943, DOI: 10.1002/elsc.201900051
Solmaz, R., 2010. Investigation of the inhibition effect of 5-((E)-4-phenylbuta-1,3-dienylideneamino)-1,3,4 thiadiazole-2-thiol schiff base on mild steel corrosion in hydrochloric acid. Corros. Sci., 52, 3321-3330.
Styrylska, T., Pietraszek, J,. 1992. Numerical modeling of non-steady-state temperature-fields with supplementary data. Zeitschrift für Angewandte Mathematik und Mechanik, 72, T537-T539
Ulewicz, R., 2015. Hardening of steel X155CrVMo12-1 surface layer. Journal of the Balkan Tribological Association, 21, 166-172.
Wójcicka K., 2021. The efficiency of municipal sewage treatment plants inspiration for water recovery. Technical Transactions 118, art. e2021023, DOI: 10.37705/TechTrans/e2021023

添加 Al_2O_3 的 WC-Co 涂层的性能

關鍵詞
软钢
电火花沉积
WC-Co-Al_2O_3涂层
特性
耐腐蚀性能

摘要
在酸性氯化物溶液中检查了 C45 低碳钢表面添加 Al_2O_3 的 WC-Co 涂层的性能。 钢表面上的 WC-Co-Al_2O_3 涂层是通过电火花（ESD）技术沉积的。 涂层的防腐性能主要采用电化学方法进行研究。 此外，扫描电子显微镜（SEM）被用于观察材料的表面。 涂层的结构取决于电火花电极的成分。 在 WC80-Co5-$Al_2O_3$15 涂层中，显示出最大的耐腐蚀性。 试样的腐蚀速率大约比未添加 Al_2O_3 的涂层小八倍。 该研究的目的是通过添加氧化铝来改善通过 ESD 方法生产的 WC-Co 涂层的功能特性。 由于 ESD 涂层的原有特性，它们可用于滑动摩擦副和切削工具上的抗磨损涂层。